NASA/TM—2015-218863

Thermal Conductivity and Erosion Durability of Composite Two-Phase Air Plasma Sprayed Thermal Barrier Coatings

Michael P. Schmitt
The Pennsylvania State University, University Park, Pennsylvania

Amarendra K. Rai
UES Inc., Dayton, Ohio

Dongming Zhu
Glenn Research Center, Cleveland, Ohio

Mitchell R. Dorfman
Oerlikon Metco Inc., Westbury, Ohio

Douglas E. Wolfe
The Pennsylvania State University, University Park, Pennsylvania

November 2015

NASA STI Program . . . in Profile

Since its founding, NASA has been dedicated to the advancement of aeronautics and space science. The NASA Scientific and Technical Information (STI) Program plays a key part in helping NASA maintain this important role.

The NASA STI Program operates under the auspices of the Agency Chief Information Officer. It collects, organizes, provides for archiving, and disseminates NASA's STI. The NASA STI Program provides access to the NASA Technical Report Server—Registered (NTRS Reg) and NASA Technical Report Server—Public (NTRS) thus providing one of the largest collections of aeronautical and space science STI in the world. Results are published in both non-NASA channels and by NASA in the NASA STI Report Series, which includes the following report types:

- TECHNICAL PUBLICATION. Reports of completed research or a major significant phase of research that present the results of NASA programs and include extensive data or theoretical analysis. Includes compilations of significant scientific and technical data and information deemed to be of continuing reference value. NASA counter-part of peer-reviewed formal professional papers, but has less stringent limitations on manuscript length and extent of graphic presentations.

- TECHNICAL MEMORANDUM. Scientific and technical findings that are preliminary or of specialized interest, e.g., "quick-release" reports, working papers, and bibliographies that contain minimal annotation. Does not contain extensive analysis.

- CONTRACTOR REPORT. Scientific and technical findings by NASA-sponsored contractors and grantees.

- CONFERENCE PUBLICATION. Collected papers from scientific and technical conferences, symposia, seminars, or other meetings sponsored or co-sponsored by NASA.

- SPECIAL PUBLICATION. Scientific, technical, or historical information from NASA programs, projects, and missions, often concerned with subjects having substantial public interest.

- TECHNICAL TRANSLATION. English-language translations of foreign scientific and technical material pertinent to NASA's mission.

For more information about the NASA STI program, see the following:

- Access the NASA STI program home page at http://www.sti.nasa.gov

- E-mail your question to help@sti.nasa.gov

- Fax your question to the NASA STI Information Desk at 757-864-6500

- Telephone the NASA STI Information Desk at 757-864-9658

- Write to:
  NASA STI Program
  Mail Stop 148
  NASA Langley Research Center
  Hampton, VA 23681-2199

NASA/TM—2015-218863

Thermal Conductivity and Erosion Durability of Composite Two-Phase Air Plasma Sprayed Thermal Barrier Coatings

Michael P. Schmitt
The Pennsylvania State University, University Park, Pennsylvania

Amarendra K. Rai
UES Inc., Dayton, Ohio

Dongming Zhu
Glenn Research Center, Cleveland, Ohio

Mitchell R. Dorfman
Oerlikon Metco Inc., Westbury, Ohio

Douglas E. Wolfe
The Pennsylvania State University, University Park, Pennsylvania

National Aeronautics and
Space Administration

Glenn Research Center
Cleveland, Ohio 44135

November 2015

Acknowledgments

This research was sponsored by the Department of Energy (DOE) STTR under award number DE-SC0004356 (Dr. Patcharin Burke) and the Applied Research Laboratory Eric Walker Fellowship Program.

Level of Review: This material has been technically reviewed by technical management.

Available from

NASA STI Program
Mail Stop 148
NASA Langley Research Center
Hampton, VA 23681-2199

National Technical Information Service
5285 Port Royal Road
Springfield, VA 22161
703-605-6000

This report is available in electronic form at http://www.sti.nasa.gov/ and http://ntrs.nasa.gov/

Thermal Conductivity and Erosion Durability of Composite Two-Phase Air Plasma Sprayed Thermal Barrier Coatings

Michael P. Schmitt
The Pennsylvania State University
University Park, Pennsylvania 16802

Amarendra K. Rai
UES, Inc.
Dayton, Ohio 45432

Dongming Zhu
National Aeronautics and Space Administration
Glenn Research Center
Cleveland, Ohio 44135

Mitchell R. Dorfman
Oerlikon Metco, Inc.
Westbury, New York 11590

Douglas E. Wolfe
The Pennsylvania State University
University Park, Pennsylvania 16802

Abstract

To enhance efficiency of gas turbines, new thermal barrier coatings (TBCs) must be designed which improve upon the thermal stability limit of 7 wt% yttria stabilized zirconia (7YSZ), ~1200 °C. This tenant has led to the development of new TBC materials and microstructures capable of improved high temperature performance. This study focused on increasing the erosion durability of cubic zirconia based TBCs, traditionally less durable than the metastable t' zirconia based TBCs. Composite TBC microstructures composed of a low thermal conductivity/high temperature stable cubic Low-k matrix phase and a durable t' Low-k secondary phase were deposited via APS. Monolithic coatings composed of cubic Low-k and t' Low-k were also deposited, in addition to a 7YSZ benchmark. The thermal conductivity and erosion durability were then measured and it was found that both of the Low-k materials have significantly reduced thermal conductivities, with monolithic t' Low-k and cubic Low-k improving upon 7YSZ by ~13 and ~25%, respectively. The 40 wt% t' Low-k composite (40 wt% t' Low-k – 60 wt% cubic Low-k) showed a ~22% reduction in thermal conductivity over 7YSZ, indicating even at high levels, the t' Low-k secondary phase had a minimal impact on thermal in the composite coating. It was observed that a mere 20 wt% t' Low-k phase addition can reduce the erosion of a cubic Low-k matrix phase composite coating by over 37%. Various mixing rules were then investigated to assess this non-linear composite behavior and suggestions were made to further improve erosion durability.

1.0 Introduction

As the demand continues for increased turbine inlet temperatures for gas turbine engines, so does the demand on the thermal barrier coating (TBC) system used to protect the engine components. Current state of the art 7 wt% yttria stabilized zirconia (7YSZ) based TBCs have reached their thermal stability limit of ~1200 °C. Operating at temperatures beyond 1200 °C for prolonged periods of time will cause the metastable t' phase to decompose into equilibrium cubic and tetragonal phases, the latter of which undergoes a phase change to monoclinic upon cooling. This phase change is accompanied by a large volumetric expansion of ~5 percent or more which causes high stresses and eventually, spallation of the coating. Additionally, bond coat and substrate materials have nearly reached their peak operating temperatures which itself can cause spallation (Ref. 1), and so to maintain bond coat/substrate temperatures, the thermal conductivity of next generation high temperature TBCs must be reduced.

The TBC literature has investigated a variety of new TBC materials (Refs. 2 to 11) including aluminates, perovskites, rare earth (RE) modified "co-doped" zirconia and the rare earth pyrochlores, as well as microstructural design architecture advancements (Refs. 12 to 16). The majority of recent research has focused on the rare earth modified zirconias and rare earth pyrochlores. Co-doped YSZ utilizes multiple rare earths to stabilize the tetragonal phase. The heavier rare earths efficiently scatter phonons while certain combinations have been shown to create immobile defect clusters (Refs. 7 and 8) which have the additional benefit of reduced sintering rates. The thermal phase stability limits of rare earth modified YSZ materials have not been evaluated to the same degree as 7YSZ, but they presumably have slightly higher temperature thresholds. This is a product of the diffusion controlled nature of the equilibrium transformation in which the defect clusters reduce diffusion and thus increase stability. However, there is no detailed published data on this matter. Rare earth pyrochlores based on zirconia have gained attention in the past few years due to their high thermal stability (Refs. 3 and 4), calcium-magnesium-alumino-silicate resistance (CMAS) (Refs. 17 and 19), and very low thermal conductivities (Refs. 4 to 6). The $RE_2Zr_2O_7$ pyrochlores possess a defect fluorite crystal structure wherein the cation site is ordered with a RE replacing the Zr on every other site. Ordered oxygen vacancies are also present on the 8a Wyckoff position. The large number of oxygen vacancies, combined with the large difference in both mass and radius between the cation species yields very low thermal conductivities. With $Gd_2Zr_2O_7$ stable in the pyrochlore phase through 1550 °C and $La_2Zr_2O_7$ stable up to 2300 °C, these materials present attractive alternatives to 7YSZ. Unfortunately, high dopant cubic low-k and pyrochlore zirconate thermal barrier coatings suffer from high erosion rates and short thermal cyclic lives due to their inherently low fracture toughness, resulting in poor overall durability. Thermal cyclic life is important to the coating lifetime estimation, while high erosion rates preclude consideration of TBCs as prime reliant systems. To improve TBC durability, the thermal cycling behavior, erosion behavior, and other factors effecting durability such as CMAS resistance, must all be understood. The thermal cyclic durability of t' and cubic low-k as well as pyrochlore TBCs (with or without YSZ layers) has been extensively studied and reported in the literature (Refs. 20 to 22) and therefore the effects of the rare earth dopants on thermal cyclic life is generally well understood. Additionally, much work has been done to understand the interaction of CMAS with high rare earth containing coatings and the resultant coating properties (Refs. 17 to 19 and 23). However, the effect of rare earth dopants on the erosion aspect of durability has not been heavily investigated in the literature. This study aims to investigate these effects.

Clearly, there is no substitute material which exhibits all the necessary properties: low thermal conductivity, high temperature stability beyond 1500 °C, and high durability. Rather than develop another class of materials, a different approach is to combine the beneficial aspects of two separate materials into one composite. With this in mind, air plasma spray (APS) composite coatings have been deposited using a low thermal conductivity/high thermal stability 'cubic Low-k' matrix phase (ZrO_2: $6Y_2O_3 – 2Gd_2O_3 – 2Yb_2O_3$ {mol %}) and a t' Low-k toughening secondary phase (ZrO_2: $2Y_2O_3 – 1Gd_2O_3 – 1Yb_2O$ {mol %}). The erosion and thermal conductivity of these composites were then determined and compared to a 7YSZ baseline.

2.0 Experimental Procedure

Powders were provided by Oerlikon Metco and mixed according to the weight fractions listed in Table 1. HVOF NiCoCrAlY (Oerlikon Metco–A386-2) bond coatings were sprayed onto 2.54 cm diameter by 0.32 cm thick buttons composed of René N5 and Mar-M-247. René N5 substrates were used for thermal conductivity testing as they are most reflective of the engine component and perform slightly better in the oxidative environment. Mar-M-247 were used for the remaining testing and characterization as they are lower cost substrates and have no change on the resulting TBC microstructure. Three topcoat powders were used in this study; a high thermal stability/low durability rare earth modified cubic zirconia (herein referred to as cubic Low-k), a lower thermal stability/high durability rare earth modified t' zirconia (herein referred to as t' Low-k), and a baseline 7 wt% yttria stabilized zirconia (7YSZ). Coatings were deposited with each of the three single phase powders and multiphase composite coatings were deposited with the three t' Low-k and cubic Low-k powder mixtures given in Table 1 for a total of six separate TBCs. Thin (~25 μm) layers of YSZ were sprayed prior to the deposition of the composites to prevent reaction between the Al_2O_3 TGO and higher rare earth containing cubic phase material. Though this composition may not have sufficient rare earth to react with the TGO, analogous coatings composed of pyrochlore materials would react and so a barrier layer was used to enable future comparisons of identical systems. The coatings were sprayed using a TriplexPro210 torch operating at 400 Amps and 45 NLPM of Ar/H_2 for a power of 45 kW. The standoff distance was 0.203 m and feed rates were 150 g/min.

Coatings were characterized via scanning electron microscopy (SEM – FEI Quanta 200 ESEM) and x-ray diffraction (XRD – PANalytical Empyrean) in the as-deposited state and after heat treatment in air in a box furnace at 1100 °C for 20 hr. For SEM, cross sections were mounted in epoxy and polished down to a final 45 nm colloidal silica step and subsequently gold sputtered to prevent charging. Jade 2010 software was used to perform XRD pattern analysis and whole pattern fitting. The pattern fits used JDPF 01-078-4083 for cubic Low-k and 01-070-4427 for t' Low-k. Thermal conductivity testing was performed at NASA Glenn Research Center using their high heat flux CO_2 gas laser system (Ref. 24). Briefly, the surface of the sample was heated to a preset temperature of ~1360 °C while backside cooled to ~1000 °C to maintain a gradient through the sample. Pyrometers measured surface temperatures while a reflectometer measured reflected power (loss). The measured thermal gradient and calculated heat through the sample were used in conjunction with bond coat and substrate thermal conductivities and thickness values to determine the thermal gradient through the coating. This enabled calculation of the coating thermal conductivity. Erosion testing was performed at The Pennsylvania State University using a custom erosion system, described in detail elsewhere (Ref. 25). In this case, 50 μm alumina media was accelerated to 100 m/s towards the sample surface. Erodent feed rate was 100 g/min with sample masses measured after various amounts of total erodent exposure. Steady-state erosion rates were taken to be the linear slopes observed in the coating mass loss versus mass erodent exposure, typically the last four to five data points.

TABLE 1.—COATING COMPOSITIONS AND STRUCTURE TABLE WITH RESULTING THICKNESS AND POROSITY VALUES FOR THE AS-DEPOSITED COATINGS

Matrix	Composition	Architecture	Thickness, μm	Porosity
1	YSZ	Monolithic	286±17	16%±2.5
2	t' Low-k	Monolithic	382±15	18%±1.7
3	50 t' – 50 c	Composite	304±16	20%±1.8
4	40 t' – 60 c	Composite	301±17	19%±2.8
5	20 t' – 80 c	Composite	281±17	19%±1.4
6	cubic Low-k	Monolithic	297±16	18%±1.8

3.0 Results and Discussion

3.1 As-Deposited Microstructure and Phase Composition

Scanning Electron Microscope (SEM) micrographs of the as-deposited single phase coatings are presented in Figure 1(a) to (d) with corresponding coating thickness and porosity values given in Table 1. Porosity is consistent through each of the coatings and is ~16 to 18 percent via image analysis (GIMP 2). The microstructures show a splat like lamellar morphology, typical of APS coatings, and with no vertical segmentation cracks. A representative higher magnification view of the t' Low-k monolithic coating is provided in Figure 1(d) which shows the significant microcracking present in these as-deposited coatings. Microcracks are beneficial in reducing the overall thermal conduction of the system and can provide strain relief during thermal cycling. However, from an erosion perspective, they can serve as stress concentrators and induce cracking and crack coalescence in the material, resulting in higher rates of erosion. It is worth noting that these microcracks are apparent in each of the three monolithic coatings.

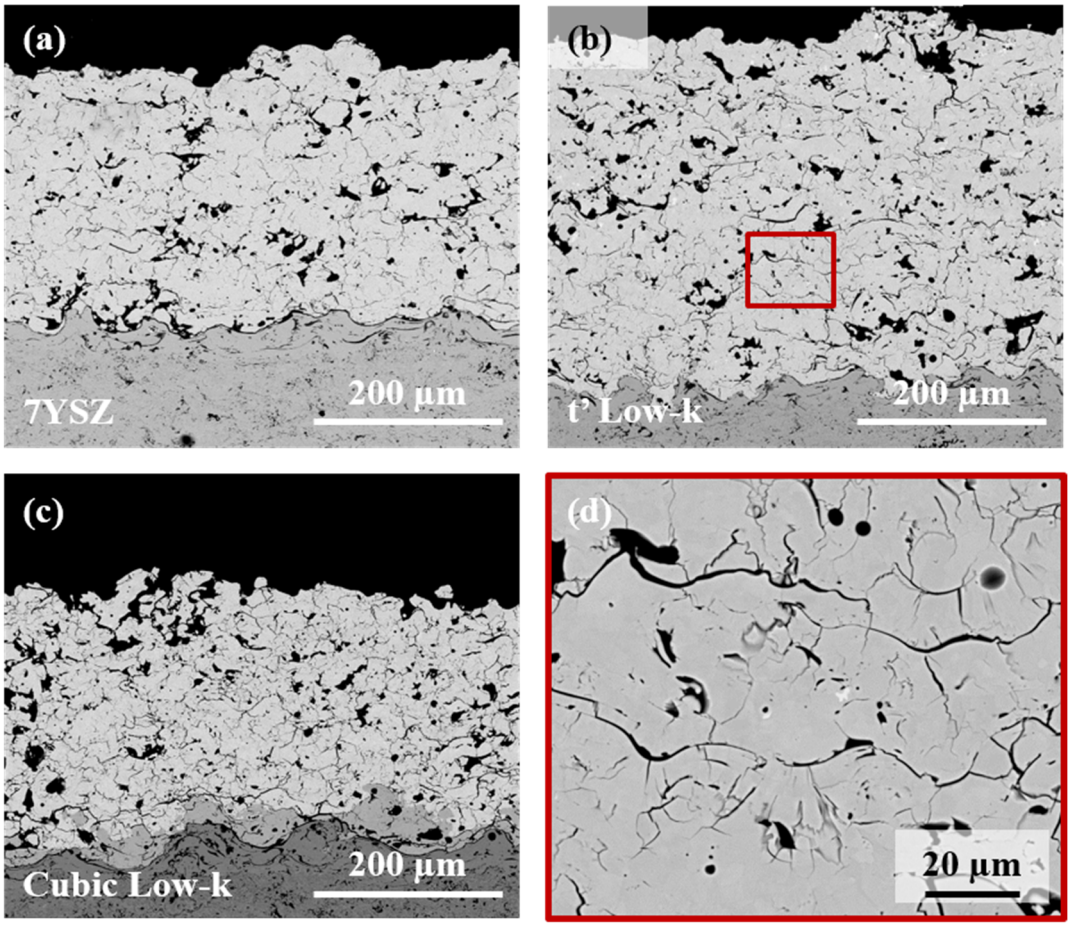

Figure 1.—SEM micrographs of the as-deposited monolithic coating polished cross sections composed of (a) 7YSZ, (b) t' Low-k, (c) and cubic Low-k showing similar porosities and morphologies. A higher magnification view of the t' Low-k coating is shown in (d) where we can see significant microcracking throughout.

SEM micrographs of composite coatings composed of 20, 40, and 50 (wt%) t' Low-k phase are shown in Figure 2(a) to (d). These composite coatings also show the standard lamellar microstructure exhibiting consistent porosity values similar to those of the parent single phase coatings, 16 to 18%. In Figure 2(a) to (d), the dark contrast of the t' Low-k phase appears uniformly distributed throughout the coatings indicating good mixing and a homogeneous distribution, both vertically and laterally. Homogenous mixing is crucial to ensuring the observed behaviors are a result of the mixing ratios and not local differences in microstructure and phase due to deposition process variability. The consistency of microstructural features among these coatings is therefore important, as it enables direct comparison of their properties as a function of phase fraction. Figure 2(d) shows a high magnification view of the 20% t' Low-k composite coating, where we can see significant microcracking in the bright cubic Low-k phase, but minimal cracking in the darker t' Low-k phase. This suggests some stress modification is occurring in the material, as the t' Low-k monolithic phase showed extensive microcracking, and thus the lack of cracking cannot purely be attributed to it being a tougher phase.

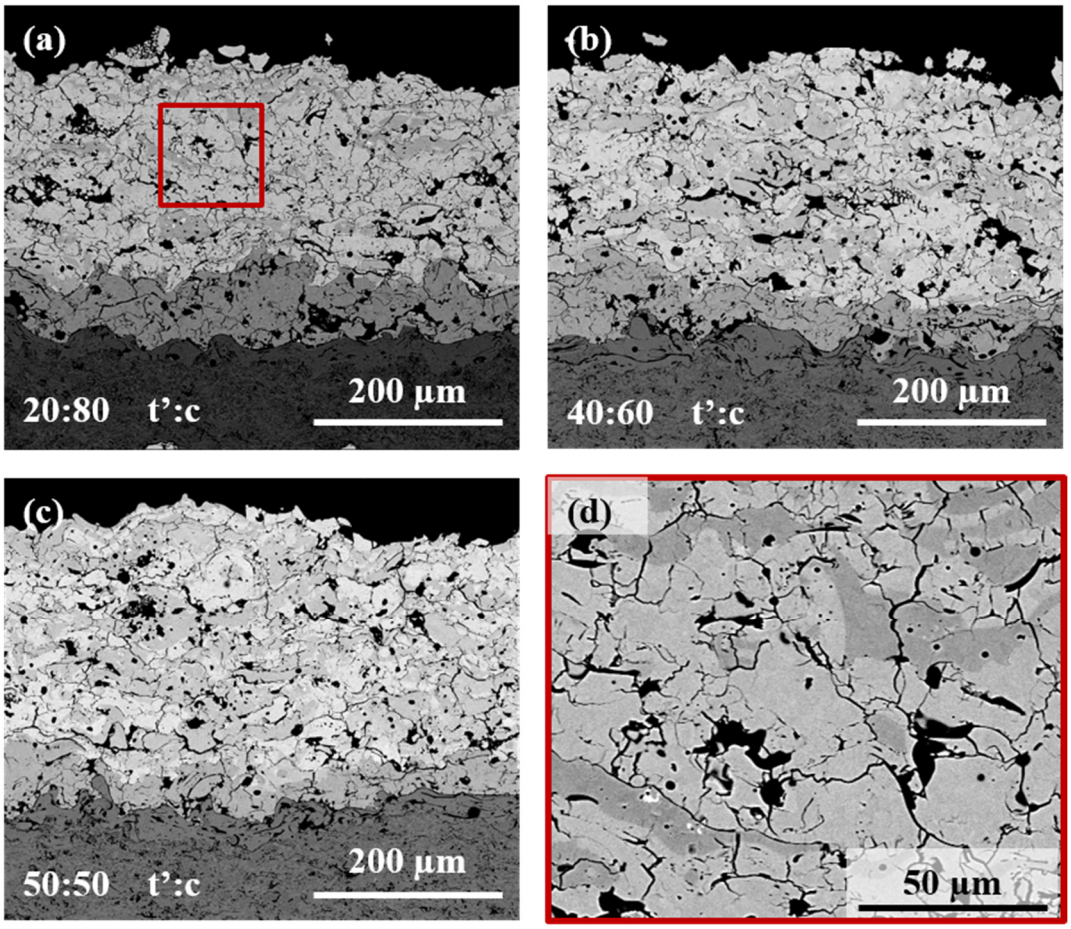

Figure 2.—SEM micrographs of the as-deposited composite coatings composed of (a) 20 wt%, (b) 40 wt%, (c) and 50 wt% t' Low-k phase showing similar porosities and morphologies. A higher magnification view of the 20 wt% t' Low-k coating is shown in (d) where we can see significant microcracking in the bright cubic phase, while the t' phase has a significantly lower crack density, suggesting modifications of the stress fields have occurred as the t' Low-k monolithic coating did exhibit microcracking.

The x-ray diffraction patterns for these coatings are presented in Figure 3(a) and (b), with the full patterns provided in Figure 3(a) and the (400)/(004) peak regions are shown in Figure 3(b). There is a trend of reducing cubic intensity and increasing tetragonal peak intensity with increasing t' Low-k additions. The cubic Low-k and t' Low-k single phase coatings show the appropriate cubic and tetragonal symmetries, with the t' Low-k coating having a nearly identical lattice parameter to YSZ (Table 2). Whole pattern fits were obtained for these coatings with the resultant lattice parameter and phase fractions (wt%) provided in Table 2. The composite coatings show a mixture of t' and cubic phases which match fairly well with the intended mixture ratios.

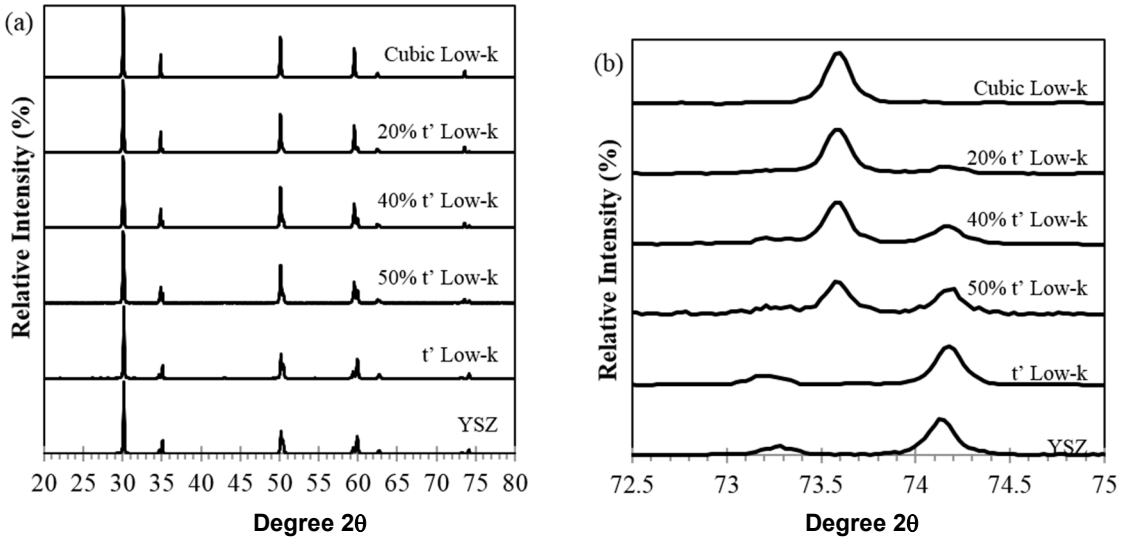

Figure 3.—XRD patterns of Matrix 1–6 with (a) showing the full patterns which show minimal preferred orientation and (b) the (004)/(400) region in which we can see the reduction in the cubic phase signal with concomitant increase in the t' signal as we add t' Low-k to the composite.

TABLE 2.—XRD WHOLE PATTERN FIT RESULTS FOR PHASE FRACTIONS (wt%) OF THE CUBIC AND TETRAGONAL PHASES FOR THE AS-DEPOSITED COATINGS BEFORE AND AFTER HEAT TREATMENT AT 1100 °C FOR 20 HR

Coating	wt% t' phase (Pre heat treat)	wt% cubic phase (Pre heat treat)	wt% t' phase (Post heat treat)	wt% cubic phase (Post heat treat)
YSZ	100	0	100	0
t' Low-k	100	0	100	0
50 t' – 50 c	56	44	54	46
40 t' – 60 c	46	54	47	53
20 t' – 80 c	22	78	23	77
cubic Low-k	0	100	0	100

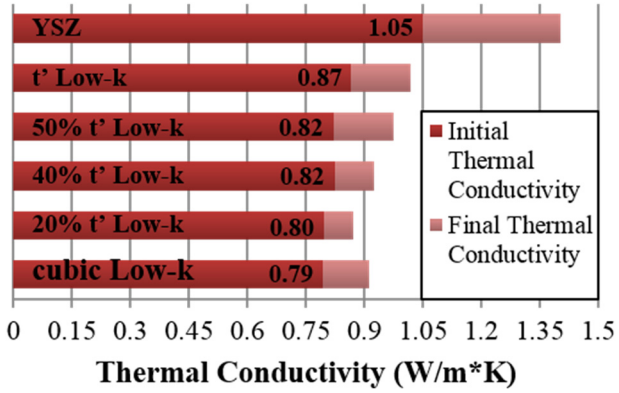

Figure 4.—Thermal conductivity of monolithic and composite t' and cubic Low-k APS TBCs with a 7YSZ reference. The dark shade represents the thermal conductivity in the as-deposited condition while the lighter shade represents the thermal conductivity after testing for 10 hr at temperature (the sintered thermal conductivity).

3.2 Thermal Conductivity

The thermal conductivities of the samples are plotted in Figure 4. The darker shade represents the as-deposited thermal conductivity value while the lighter shade represents thermal conductivity after 10 hr of testing. Of the monolithic coatings, the YSZ sample had the highest initial (1.05 W/m*K) and final (1.40 W/m*K) thermal conductivities while the cubic low-k sample had the lowest initial (0.79 W/m*K) and final (0.91 W/m*K) thermal conductivities. The t' Low-k sample exhibited initial (0.87 W/m*K) and final (1.02 W/m*K) thermal conductivities between that of cubic low-k and YSZ. This behavior is expected due to the heavier rare earths present in the t' Low-k and cubic Low-k materials (compared to Y) which have a higher mass contrast with Zr and thus enhanced phonon scattering. In the cubic Low-k, the higher overall rare earth content results in a higher concentration of charge compensating oxygen vacancies which further inhibits phonon transport. The increase in thermal conductivity for both cubic Low-k (~12%) and t' Low-k (~15%) materials is significantly lower than that of YSZ (~35%). The increase in thermal conductivity is typically attributed to sintering, however phenomena such as delamination, phase change, and compositional change can also play an important role. Delamination or cracking often leads low thermal conductivity values due to lack of heat transport through the crack or delamination. In our case, no delaminations were witnessed for these samples due in part to the low interface temperatures of ~1000 °C. It should be noted that the YSZ sample surface temperature was slightly higher than the other samples at ~1400 °C which could have slightly inflated the increase in thermal conductivity with respect to the other samples. Thermal conductivity values for the composite coatings increase as t' content increases with values of 0.80, 0.82, and 0.82 W/m*K at 20, 40, and 50% t' phase. The lack of change between the 40 and 50% t' Low-k composites is due to the small change 10% change in weight fraction corresponding to a small change in thermal conductivity, i.e., the thermal conductivity difference between cubic and t' Low-k is only 0.08 W/m*K so a 10% change is only 0.008 W/m*K. This, combined with the inherent uncertainty in the measurement due to thickness and experimental error make resolution difficult at these levels. The rate of thermal conductivity increase also increases with t' Low-k content in the composite coatings, however it appears that small additions of t' secondary phase have reduced the rate compared to pure cubic phase coatings. This could be an effect of slight differences in splat boundary behavior. Overall, the composite coatings provide beneficial reductions in thermal conductivity, with values favoring the cubic Low-k matrix phase even at high amounts of t' Low-k secondary phase, all while minimizing increase in thermal conductivity. The thermal conductivity and rate of thermal conductivity increase of the composites are both significantly lower than a standard 7YSZ benchmark.

TABLE 3.—EROSION RATES FOR COATINGS IN THE AS-DEPOSITED STATE
AND AFTER HEAT TREATMENT AT 1100 °C FOR 20 HR
[Percentage reductions from the as-deposited to post heat treatment are given in the last column.]

Coating	As deposited erosion rate ($g/kg*10^{-1}$)	Post heat treat erosion rate ($g/kg*10^{-1}$)	Percent reduction in erosion rate
YSZ	1.357	0.689	49
t' Low-k	1.431	0.649	55
50 t' – 50 c	3.057	1.962	36
40 t' – 60 c	3.987	2.235	44
20 t' – 80 c	4.579	3.228	30
cubic Low-k	6.481	4.435	32

3.3 As-Deposited Erosion Behavior

The steady state erosion rates for these coatings were calculated from the slope of the linear portion of coating mass loss versus mass erodent exposure graphs which were typically the last four to five data points, and these results are presented in Table 3. Initial data points include surface contributions such as roughness, and though valuable in some cases, do not represent a steady erosion rate and were not included in this study. Table 3 contains erosion data for both the as-deposited state as well as after heat treatment at 1100 °C for 20 hr. It is often overlooked that the mass loss does not always truly represent how fast a coating is being degraded, i.e., a material with a higher theoretical density may have the same mass loss rate as a lighter material, yet its volume loss rate is significantly lower. Therefore, in cases where the bulk density of the materials or porosity of the coatings being compared is significantly different, then comparing mass loss rates may be an improper assessment, and thus the data must be normalized. In the current study, the porosity is similar in each of the coatings and the cubic and tetragonal phases have similar bulk densities (~6.1 vs. ~6.00 g/cc, respectively) that the mass loss rate may be used as a sufficient comparison. From Table 3, the erosion rates of YSZ and t' Low-k are within 5% of each other and are significantly lower than cubic Low-k. As expected, additions of the t' phase in the composite coatings reduce the erosion rate with respect to the cubic matrix. However, the relationship is not linear; at 50 wt% t' phase content, the erosion rate is well below 50% of the difference between cubic Low-k and t' Low-k erosion rates. The same behavior is also observed for the 20% and 40% t' containing composites.

To better understand the effects of the t' additions, we can borrow from composite literature and apply various mixing rules (Refs. 26 to 28). Figure 5 depicts the upper (Fig. 5(a)) and lower (Fig. 5(b)) boundary behavior with a simplified laminar composite composed of one layer of material-a sandwiched between two layers of material-b. The upper boundary for mixing behavior is described by parallel or linear mixing where the stress is aligned in the plane of the lamellae. Assuming good bonding between the layers ($\varepsilon_a = \varepsilon_b$), then we can apply Hooke's law and a force balance to arrive at Equation (1) for linear mixing:

$$E = E_a f_a + E_b f_b \tag{1}$$

where E is the modulus of the composite, E_a and E_b are the modulus of material-a and material-b, and f_a and f_b are the volume fraction of material-a and material-b, respectively. In Figure 5(b) we see the case for the lower boundary mixing in which case the stresses are equal in both materials ($\sigma_a = \sigma_b$). Using the same parameters, the lower boundary is therefore described by series mixing (Eq. (2)):

$$E^{-1} = \frac{f_a}{E_a} + \frac{f_b}{E_b} \tag{2}$$

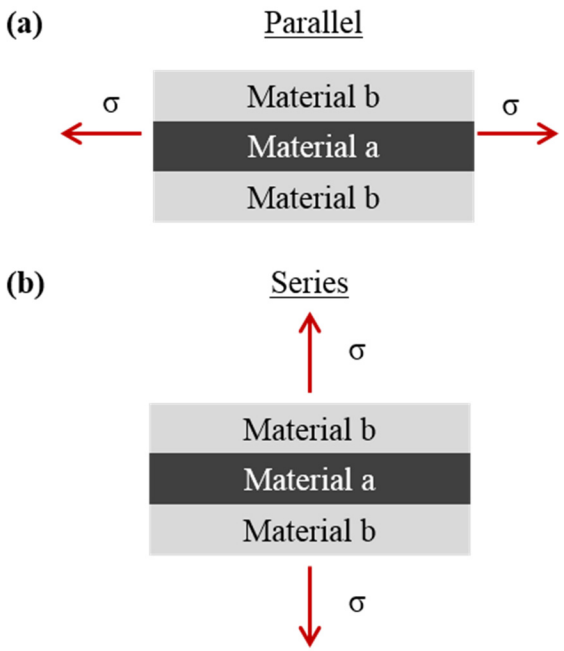

Figure 5.—Schematic showing (a) parallel behavior where the tensile stress is aligned along the plane of the composite layers and strains are assumed equivalent in both materials and (b) stress is normal to the composite layers and stresses are assumed equivalent in both materials. The parallel case allows for a high modulus phase to withstand a larger degree of the force, and thus toughen the material.

Often, real composites are a function of both types of behavior and so are described by logarithmic equations (Eq. (3)):

$$E = e^{fa \ln E_a + b \ln E_b} \tag{3}$$

The last function investigated is the Halpin-Tsai mixing rule which utilizes a fitting parameter (ξ) that can describe the degree of parallel or series behavior. When the value of $\xi = 0$, the Halpin-Tsai equation simplifies to the series rule and when the value of $\xi = \infty$ (or a large number), the Halpin-Tsai equation simplifies to the parallel rules. The general rule is given below (Eq. (4)):

$$E = \frac{(1 + \xi \eta f_a)}{(1 - \eta f_a)} E_b \quad \text{where } \eta = \frac{(E_a - E_b)}{E_a + \xi E_b} \tag{4}$$

These mixing rules relate the modulus of the composite to the modulus of the individual phases, however, we are most interested in understanding the erosion behavior of our material. Unfortunately, there is no strict mechanics based formulae in which we can arrive at Equations (1) to (4) in terms of erosion rates. However, using a few assumptions we can relate the erosion rate to these equations. From Aquaro and Fontani (Ref. 29), elastic theory shows that the volume (V) of material removed (i.e., the erosion rate) during erosion of brittle ceramics is inversely proportional to K_{Ic}, as shown below (Eq. (5)):

$$V \propto w_p^{21/10} R_p^{11/3} \rho_p^{21/20} K_{Ic,t}^{-4/3} H_t^{-1/4} \tag{5}$$

where w_p is the velocity of the particle, R_p is the radius of the particle, ρ_p is the density of the particle, $K_{IC,t}$ is the fracture toughness of the target (coating), and H_t is the hardness of the target (coating). The stress intensity factor, K, is a description of the stress state at the crack tip. K_c is the critical stress intensity required to propagate a crack and is frequently used in fracture mechanics to describe the toughness of a material. For a Penny-shaped crack in an infinite domain, Equation (6) for mode *I* stress intensity holds:

$$K_I = 2\sigma\sqrt{\frac{a}{\pi}} \tag{6}$$

where σ is the stress and (a) is the crack radius. Rearranging and substituting K_{Ic} yields an equation for a critical stress, σ_{crit}, beyond which a mode *I* crack will propagate in a material:

$$\sigma_{crit} = \frac{K_{Ic}}{2}\sqrt{\frac{\pi}{a}} \tag{7}$$

Equations (6) and (7) can then be substituted into the K_{Ic} term in Equation (5) and rearrange to yield a proportionality for stress relating to volume loss (Eq. (8)):

$$\sigma_{crit} \propto \sqrt{\frac{\pi}{4a}}\frac{1}{V^{3/4}} \tag{8}$$

where volume loss, and therefore erosion rate, is inversely proportional to the stress. Through Hooke's law, Equations (1) to (4) are valid in terms of stress, and therefore can be written in terms of the inverse erosion rate. There would of course be a proportionality constant which would incorporate impingement angle, velocity, hardness, mass, etc., however this is outside the scope of this study where the primary concern is the applicability of the mixing laws to erosion rates. In this manner, we can then link the inverse erosion rates to the mixing equations. Using this relation, Figure 6 plots the as-deposited inverse erosion rates for each coating along with the predicted profiles using Equations (1) to (4). The y-axis then corresponds to increasing toughness values (lower erosion rates). Comparing the data to the various mixing equations enables a better understanding of how compositional changes affect composite behavior

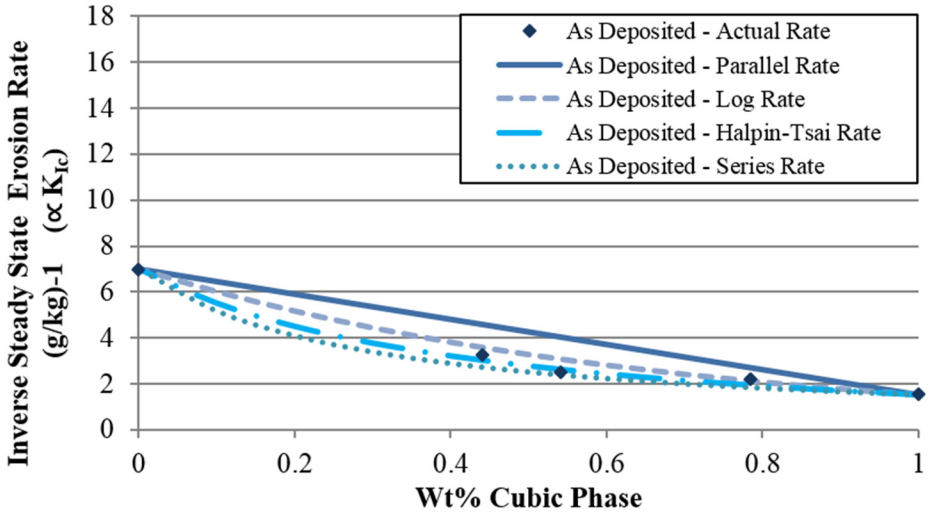

Figure 6.—The inverse steady state erosion rates of the composite coatings in the as-deposited state as a function of the wt% cubic phase, along with plots for parallel, log, Halpin-Tsai and Series mixing rules. The inverse of the steady state erosion rate is used, as this value is proportional to (increases with) the toughness of the coating, which can be related to the stresses and therefore the mixing equations.

for APS coatings. It is immediately apparent that the data is near the series boundary, indicating series mixing behavior. Since series behavior indicates the two phases experience roughly equal impact stresses, this suggests minimal toughening effects. A good Halpin-Tsai fit was obtained for $\xi = 0.5$, further indicating numerically the degree of series behavior as a $\xi = 0$ simplifies to series. From Figure 6, for any fraction of cubic phase the inverse erosion rate (toughness) is higher in the parallel case and thus ideal behavior is characterized by parallel mixing. This is attributed to the parallel case allowing for unequal stresses to be present in the two phases, and so the phase with the higher toughness, and therefore larger σ_c, could in theory carry more of the load. The composites do exhibit some parallel behavior since they are inside the series boundary; however, there is significant room for improvement. As the mixing behavior is generally dictated by the alignment of the stresses and the composite phases, modifications could be made to better align the stress with the microstructure to enable parallel type behavior. This will be discussed in further detail in section 3.5.

3.4 Post Heat Behavior

To determine the effects of elevated temperature on erosion performance, these coatings were isothermally heat treated to 1100 °C for a period of 20 hr. Though higher temperatures would perhaps be more representative of engine operating conditions and are indeed the goal of these coatings, a slightly lower temperature was used due to the isothermal nature of the heat treatment and the need to maintain bond coat/substrate integrity. X-ray diffraction showed effectively no phase fraction changes from the as-deposited conditions suggesting minimal destabilization or interaction in the region probed. Though the cubic Low-k phase has a higher rare earth content, the resulting concentration gradient is not sufficient to yield significant interdiffusion at these temperatures. Additionally, the time at this temperature is not sufficient to destabilize the t' phase. Overall, this results in minimal changes in phase fractions. The erosion rates provided in Table 3 are significantly lower for the heat treated coatings. This is attributed to the annealing of microcracks and splat boundaries resulting in sintering and densification and thus improved toughness, as has been observed by others (Ref. 30). The inverse erosion rates for the heat treated coatings are presented in Figure 7 using Equations (1) to (4). As toughness values have likely increased due to sintering of flaws and defects, so have the inverse erosion rates, with the experimental data just inside the series boundary. Figure 7 confirms excellent agreement with the Halpin-Tsai equation when $\xi = 0.5$. It appears that while the heat treatment reduced the erosion rates, the erosive mechanism

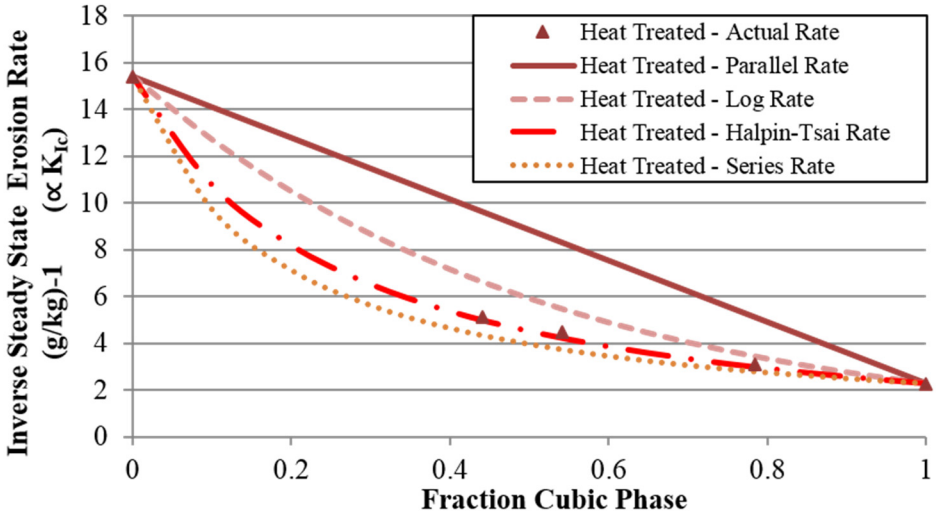

Figure 7.—The inverse steady state erosion rates of the composite coatings after heat treatment at 1100 °C for 20 hr a function of the wt% cubic phase, along with plots for parallel, log, Halpin-Tsai and Series mixing rules. The inverse of the steady state erosion rate is used, as this value is proportional to (increases with) the toughness of the coating, which can be related to the stresses and therefore the mixing equations.

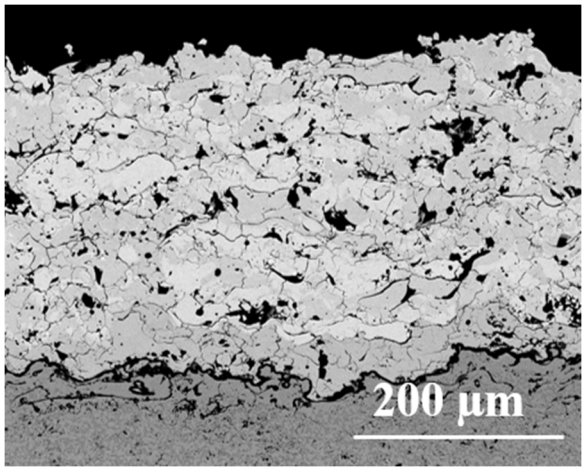

Figure 8.—SEM image of the 50% t' Low-k coating after heat treatment at 1100 °C for 20 hr. Aside from some sintering of microcracks and smaller splat boundaries, there is minimal change in the overall microstructure.

and behavior have remained unchanged for the APS composite coatings. This is supported by Figure 8 which shows no change in the 50% t' Low-k coating morphology; aside from sintering effects such as annealing microcracks, the heat treatment did not drastically change the microstructure (i.e., grain size and morphology) and so the overall behavior remained similar for the composite TBCs. Notably, the percent reduction in erosion rate does not correlate with the percent increase in thermal conductivity, even though both are typically attributed to sintering. In Table 3 and Figure 4, the t' Low-k has the largest drop in erosion rate yet has a relatively small increase in thermal conductivity. On the other hand, YSZ has a large increase in thermal conductivity, there is a smaller change in the heat treated erosion suggesting sintering is not as drastic as t' Low-k. There could be several factors for this behavior. First, the contributions of microcracks and splat boundaries are different between erosion and thermal conductivity. For thermal conductivity, the splats are primarily aligned horizontally and are thus the major contributor to the reduction in heat transport. The microcracks however, are not primarily horizontally aligned and are therefore not as effective in reducing thermal conduction, and thus not a large contributor to thermal conduction. In comparison, during erosion, the particle impact causes a stress wave that propagates in all directions from the center of the impact. Therefore, microcracks aligned in any direction could potentially cause increases in local stress intensity depending on the impact and stress wave direction, i.e., as long as the impact occurs in the right location, the stress wave could be perpendicular to the crack. This is in contrast to thermal conductivity, where only the horizontal aspect of microcracks has an impact on performance. As a result, microcrack features have a larger contribution to the erosion performance as they have an effect on stress intensity regardless of orientation/alignment and can easily "link-up" to create large cracks or connect splat boundaries resulting in increased erosion. The degree of microcracking is difficult to quantify and could have varied between these coatings resulting in unexpected degrees of change in erosion rate. Additionally, the heat treat performed prior to erosion was at 1100 °C while the thermal conductivity was a ~1360 °C gradient test. It is clear the effect of a heat treatment and densification may therefore be different between the two tests, but is well outside the scope of this effort. The most important takeaway however, is that regardless of testing method the composite behavior remains intact after heat treatment. This is vital for ensuring erosion durability of coatings which will experience long durations at elevated temperature.

3.5 Improvement of Phase Mixing and Non Ideal Behavior

Initial results in Table 3 show some benefit beyond simple linear trends in erosion rate yet composite mixture rules indicated much more benefit could be derived. It is clear that parallel mixing behavior is ideal, both fundamentally due to the ability to promote unequal stresses (Fig. 5) as well as hypothetically, where the mixture rules suggest higher toughness (inverse erosion rate) for the parallel case (Figs. 6 and 7). Therefore, to maximize the benefit of the t' phase on coating performance, the t' phase must be properly aligned with the stresses. Though the stress fields cannot be controlled, the microstructure can. Thus, it is ideal to align the microstructure as favorably as possible with the impact stresses. The stress fields under a spherical elastic contact has been described by Fischer-Cripps using cylindrical polar coordinates due to the symmetrical nature of the contact (Ref. 31). From their plots of principle stress (σ_1 and σ_3) contours and trajectories, a compressive stress field is observed to emanate from beneath the contact in a direction normal to the contact (Fig. 5.4.3 in Ref. 31). Meanwhile, a tensile field initiates just outside the contact area and radiates outward. This tensile field is responsible for the typical Hertzian cone behavior in ceramics and is largest in magnitude near the surface of the contact. Since tensile stresses are the primary driving force for cracking, the trajectory of the largest tensile stresses are particularly important, i.e., those near the surface. The directionality of those stresses is shown in the trajectory plots and it is observed that the tensile forces near the surface are acting effectively in-plane, parallel to the surface. As previously discussed, the ideal composite behavior is when the stresses are aligned parallel to the individual composite layers. Thus, it is crucial that the splat lamellae (layers) are aligned parallel to the surface in order to maximize toughening.

Two other important factors to consider are related to the non ideal nature of mixing laws relating to real materials: flawed microstructure and non uniaxial loading. In the parallel behavior, the mixing laws assume perfect bonding between the two materials or phases, thus enabling the strains to be equivalent. In a real material, perfect bonding is rarely the case. This is especially true for a highly defective APS coating which contains significant inter-lamellar porosity, regions of poorly bonded particles and interfaces, microcracking, and general porosity throughout. These flaws function as stress concentrators and immediate crack pathways, and importantly for mixing, poorly bonded regions. The stress concentrators can cause higher stresses to occur in the lower toughness cubic Low-k phase of the composite coating and thus reduce the effectiveness of the toughening t' Low-k phase. Even in the ideal case of stresses aligning parallel to the lamellae, if the two phases are poorly bonded the weaker phase may not be shielded from the stresses well enough, resulting in failure. Thus, even if the microstructure is properly aligned with the stresses, the flaws inherent to the APS microstructure may diminish the toughening effects. Additionally, the second important factor is the assumed uniaxial loading used in composite mixture rules versus the non-ideal shear stresses imparted by particles. This issue is compounded when considering the flawed nature of these coatings and that the already weak splat boundaries could be further weakened or even fractured by shear stresses. These contributions are not incorporated in the simple mixture rules but are extremely relevant in real materials, particularly in defective APS coatings.

4.0 Conclusions

To function at operating temperatures higher than currently achieved, future TBCs must possess lower thermal conductivities while maintaining thermochemical stability, and improved overall durability (i.e., erosion durability and thermal cyclic life). No current material satisfies all of these criteria, for example, the rare earth pyrochlores exhibit the required thermal properties but lack the necessary mechanical properties for high overall durability. This work suggests that composite t' and cubic Low-k coatings have the potential to improve TBC performance by utilizing a toughening t' Low-k phase to impart erosion durability to an otherwise thermally stable, low conductivity cubic Low-k matrix phase. It has been shown that the thermal conductivities of these t' Low-k/cubic Low-k composite coatings are significantly lower than 7YSZ while maintaining comparable porosity and morphology. It was also

observed that additions of t' Low-k secondary phases can improve the erosion durability of a cubic Low-k coating in a non-linear fashion. A 20% addition of t' Low-k phase decreased the erosion rate by more than 37% of the difference between t' Low-k and cubic Low-k. Composite mixing rules have suggested there is even more room for improvement and that increased benefit can be derived from tailored microstructures of composite TBCs.

Though parallel mixing provides a fundamental limit to the benefits of the secondary phase, the practical benefits in real materials are limited by flaws and defects combined with the directionality of the impact stress fields. Future work could focus on achieving these practical limits via microstructural modifications to maximize the toughening effect of secondary phases when experiencing particle impacts by promoting lamellar that are primarily aligned planar to the surface. By maximizing the effect of the secondary phase, the volume fraction (and therefore any deleterious behavior) can be minimized. Also, though this work utilized a toughening t' Low-k phase which may be unstable at elevated temperatures (>1400 °C) for prolonged periods, it lays the groundwork for future studies with other secondary phases which are thermally stable in this temperature range. In the practical case, the secondary phase must have high overall durability and thermal stability but does not necessarily need low thermal conductivity as the matrix phase provides the bulk of the thermal insulation. This opens up a variety of materials not traditionally considered for TBC applications. Additionally, future work will focus on investigating the thermal cyclic lives to gain a better picture of the overall durability of these coatings.

References

1. A.G. Evans, D.R. Mumm, J.W. Hutchinson, G.H. Meier, F.S. Pettit, Mechanisms controlling the durability of thermal barrier coatings, Prog. Mater. Sci. 46 (2001) 505–553. doi:10.1016/S0079-6425(00)00020-7.
2. D.R. Clarke, C.G. Levi, Materials Design for the Next Generation Thermal Barrier Coatings, Annu. Rev. Mater. Res. 33 (2003) 383–417. doi:10.1146/annurev.matsci.33.011403.113718.
3. X.Q. Cao, R. Vassen, D. Stover, Ceramic materials for thermal barrier coatings, J. Eur. Ceram. Soc. 24 (2004) 1–10. doi:10.1016/S0955-2219(03)00129-8.
4. R. Vassen, X. Cao, F. Tietz, D. Basu, D. Stover, Zirconates as New Materials for Thermal Barrier Coatings, J. Am. Ceram. Soc. 83 (2000) 2023–2028.
5. C.G. Levi, Emerging materials and processes for thermal barrier systems, Curr. Opin. Solid State Mater. Sci. 8 (2004) 77–91. doi:10.1016/j.cossms.2004.03.009.
6. N.P. Bansal, D. Zhu, Effects of doping on thermal conductivity of pyrochlore oxides for advanced thermal barrier coatings, Mater. Sci. Eng. A. 459 (2007) 192–195. doi:10.1016/j.msea.2007.01.069.
7. D. Zhu, R.A. Miller, Thermal Conductivity and Sintering Behavior of Advanced Thermal Barrier Coatings, in: H.T. Lin, M. Singh (Eds.), 26th Annu. Conf. Compos. Adv. Ceram. Mater. Struct. B Ceram. Eng. Sci. Proc., John Wiley and Sons, Inc., Hoboken, NJ, 2008: pp. 457–468.
8. D. Zhu, Y.L. Chen, R.A. Miller, Defect Clustering and Nano-Phase Structure Characterization of Multi-Component Rare Earth Oxide Doped Zirconia-Yttria Thermal Barrier Coatings, in: 27th Annu. Cocoa Beach Conf. Adv. Ceram. Compos. A Ceram. Eng. Sci. Proc., John Wiley and Sons, Inc., Hoboken, NJ, 2003: pp. 525–534.
9. D. Zhu, J.A. Nesbitt, C.A. Barrett, T.R. McCue, R.A. Miller, Furnace Cyclic Oxidation Behavior of Multicomponent Low Conductivity Thermal Barrier Coatings, J. Therm. Spray Technol. 13 (2004) 84–92. doi:10.1361/10599630418185.
10. N.P. Bansal, D. Zhu, Thermal properties of oxides with magnetoplumbite structure for advanced thermal barrier coatings, Surf. Coatings Technol. 202 (2008) 2698–2703. doi:10.1016/j.surfcoat.2007.09.048.
11. R. Darolia, Thermal barrier coatings technology: critical review, progress update, remaining challenges and prospects, Int. Mater. Rev. 58 (2013) 315–348. doi:10.1179/1743280413Y.0000000019.

12. D.E. Wolfe, J. Singh, R.A. Miller, J.I. Eldridge, D. Zhu, Tailored microstructure of EB-PVD 8YSZ thermal barrier coatings with low thermal conductivity and high thermal reflectivity for turbine applications, Surf. Coatings Technol. 190 (2005) 132–149. doi:10.1016/j.surfcoat.2004.04.071.
13. M.P. Schmitt, A.K. Rai, R. Bhattacharya, D. Zhu, D.E. Wolfe, Multilayer thermal barrier coating (TBC) architectures utilizing rare earth doped YSZ and rare earth pyrochlores, Surf. Coatings Technol. 251 (2014) 56–63. doi:10.1016/j.surfcoat.2014.03.049.
14. A.K. Rai, M.P. Schmitt, R.S. Bhattacharya, D. Zhu, D.E. Wolfe, Thermal conductivity and stability of multilayered thermal barrier coatings under high temperature annealing conditions, J. Eur. Ceram. Soc. 35 (2015) 1605–1612. doi:10.1016/j.jeurceramsoc.2014.11.003.
15. S. Gu, T.J. Lu, D.D. Hass, H.N.G. Wadley, Thermal Conductivity of Zirconia Coatings With Zig-Zag Pore Microstructures, Acta Mater. 49 (2001) 2539–2547.
16. K.D. Harris, D. Vick, E.J. Gonzalez, T. Smy, K. Robbie, M.J. Brett, Porous thin films for thermal barrier coatings, Surf. Coatings Technol. 138 (2001) 185–191. doi:10.1016/S0257-8972(00)01155-5.
17. S. Krämer, J. Yang, C.G. Levi, C.A. Johnson, Thermochemical Interaction of Thermal Barrier Coatings with Molten CaO-MgO-Al2O3-SiO2 (CMAS) Deposits, J. Am. Ceram. Soc. 89 (2006) 3167–3175. doi:10.1111/j.1551-2916.2006.01209.x.
18. S. Krämer, J. Yang, C.G. Levi, Infiltration-Inhibiting Reaction of Gadolinium Zirconate Thermal Barrier Coatings with CMAS Melts, J. Am. Ceram. Soc. 91 (2008) 576–583. doi:10.1111/j.1551-2916.2007.02175.x.
19. C.G. Levi, J.W. Hutchinson, M.H. Vidal-Sétif, C.A. Johnson, Environmental degradation of thermal-barrier coatings by molten deposits, MRS Bull. 37 (2012) 932–941. doi:10.1557/mrs.2012.230.
20. D. Zhu, R.A. Miller, Development of Advanced Low Conductivity Thermal Barrier Coatings, Int. J. Appl. Ceram. Technol. 1 (2004) 86–94. doi:10.1111/j.1744-7402.2004.tb00158.x.
21. E. Bakan, D.E. Mack, G. Mauer, R. Vaßen, Gadolinium Zirconate/YSZ Thermal Barrier Coatings: Plasma Spraying, Microstructure, and Thermal Cycling Behavior, J. Am. Ceram. Soc. 97 (2014) 4045–4051. doi:10.1111/jace.13204.
22. R. Vaßen, M.O. Jarligo, T. Steinke, D.E. Mack, D. Stöver, Overview on advanced thermal barrier coatings, Surf. Coatings Technol. 205 (2010) 938–942. doi:10.1016/j.surfcoat.2010.08.151.
23. S. Kramer, S. Faulhaber, M. Chambers, D. Clarke, C. Levi, J. Hutchinson, et al., Mechanisms of cracking and delamination within thick thermal barrier systems in aero-engines subject to calcium-magnesium-alumino-silicate (CMAS) penetration, Mater. Sci. Eng. A. 490 (2008) 26–35. doi:10.1016/j.msea.2008.01.006.
24. D. Zhu, R.A. Miller, B.A. Nagaraj, R.W. Bruce, Thermal conductivity of EB-PVD thermal barrier coatings evaluated by a steady-state laser heat flux technique, Surf. Coatings Technol. 138 (2001) 1–8. doi:10.1016/S0257-8972(00)01145-2.
25. D.E. Wolfe, M.P. Schmitt, D. Zhu, A.K. Rai, R. Bhattacharya, Multilayered Thermal Barrier Coating Architectures for High Temperature Applications, in: D. Zhu, H.-T. Lin, Y. Zhou, T. Hwang (Eds.), 37th Int. Conf. Adv. Ceram. Compos. Adv. Ceram. Coatings Mater. Extrem. Environ., John Wiley and Sons, Inc., Hoboken, NJ, 2013: pp. 3–18.
26. W. Voigt, Ueber die Beziehung zwischen den beiden Elasticitätsconstanten isotroper Körper, Ann. Phys. 274 (1889) 573–587. doi:10.1002/andp.18892741206.
27. A. Reuss, Berechnung der Fliehgrenze von Mischkristallen auf Grund der Plastizitatsbedingung fur Einkristalle., Zeitschrift Für Angew. Math. Und Mech. 9 (1928) 49–58. doi:10.1002/zamm.19290090104.
28. J.C. Halpin, Stiffness and Expansion Estimates for Oriented Short Fiber Composites, J. Compos. Mater. 3 (1969) 732–734. doi:10.1177/002199836900300419.
29. D. Aquaro, E. Fontani, Erosion of ductile and brittle materials, Meccanica. 36 (2001) 651–661. doi:10.1023/A:1016396719711.
30. R.G. Wellman, J.R. Nicholls, A review of the erosion of thermal barrier coatings, J. Phys. D. Appl. Phys. 40 (2007) R293–R305. doi:10.1088/0022-3727/40/16/R01.
31. A.C. Fischer-Cripps, Introduction to Contact Mechanics, Second Edi, Springer, New York, 2007.